MOX–Report No. 28/2010

Fluid Structure Interaction Simulations of Physiological Blood Flow in the Aorta

Paolo Crosetto, Philippe Reymond, Simone Deparis,
Dimitrios Kontaxakis, Nikolaos Stergiopulos,
Alfio Quarteroni

MOX, Dipartimento di Matematica "F. Brioschi"
Politecnico di Milano, Via Bonardi 9 - 20133 Milano (Italy)

mox@mate.polimi.it http://mox.polimi.it

Fluid Structure Interaction Simulations of Physiological Blood Flow in the Aorta

Paolo Crosetto, Philippe Reymond, Simone Deparis,
Dimitrios Kontaxakis, Nikolaos Stergiopulos, Alfio Quarteroni

September 14, 2010

Abstract

The numerical tools to simulate blood flow in the cardiovascular system are constantly developing due to the great clinical interest and to scientific advances in mathematical models and computational power. The present work aims to address and validate new algorithms to efficiently predict the hemodynamics in large arteries. The latter rely on finite elements simulation of the fluid-structure interaction between blood flow and arterial wall deformation of a healthy aorta. Different sets of boundary conditions are devised and tested. The mean velocity and pressure time evolution is plotted on different sections of the aorta and the wall shear stress distribution is computed. The results are compared with those obtained with a rigid wall simulation. Pulse wave velocity is computed and compared with the values available from the literature. The flow boundary conditions used for the outlets are obtained using the solution of as one dimensional model. The results of the simulations are in agreement with the physiological data in terms of wall shear stress, wall displacement, pressure waveforms and velocities.

1 Introduction

Blood flow dynamics in arteries is an underlying factor for many vascular pathologies. A better understanding of these dynamics could improve the prediction and diagnosis in both healthy and pathological situations [11]. A simulation with rigid walls fails to predict some essential characteristics of the blood flow (such as pressure wave propagation). Thus it cannot be considered reliable in every situation (e.g. when the vessels undergo relatively large displacements). Furthermore, in most of the physiological cases the appearance of secondary flow (because of, e.g., branching or curved arteries) makes it necessary to consider the 3D dynamics. Since this dramatically increases the computational cost, it becomes of utmost importance to develop and implement parallel and scalable computational algorithms.

Modeling the Fluid-Structure Interaction (FSI) between the blood and the arterial wall is a challenging task. The research in this field is developing fast concerning both modeling aspects and computational efficiency. Taking into account the compliance of the vessels can be achieved by introducing a 3D or 2D elastic structure, using a Lagrangian, Eulerian, or Arbitrary Lagrangian Eulerian (ALE) formulation. The structure model should take into account the non linearity due to the collagen activation and the presence of surrounding tissue inducing a static pressure and a dynamic response to the wall displacement.

Alternative options that avoid the introduction of a structure model for the external wall are transpiration techniques (e.g. [7, 6]), or the coupled momentum method, used e.g. by Kim et al. [17]. These methods consist of dropping the homogeneous Dirichlet condition at the fluid-structure interface, and substituting it with a proper condition that emulates the presence of a surrounding structure. In particular the coupled momentum method shows good results in many physiological situations, and it has the advantage of being computationally cheap because the mesh is fixed. Although it is well suited for small displacements, it can be inappropriate when the displacements become large [8]. Furthermore, as the fixed control volume where the fluid equations are solved allows the fluid to pass through the interface, the quantities computed at the boundary , such as the wall shear stress, are subject to a further approximation. The FSI simulation of blood flow in the aortic arch was performed in [13] on a simplified geometry without branching and using a three-layer nonlinear model for the structure. In [13] the FSI system is formulated in an ALE frame and solved with a standard Dirichlet-Neumann method imposing an inlet flux and homogeneous Neumann condition on the outlet. An FSI simulation in a patient-specific aorta using the ALE formulation can be found in Bazilevs et al. [3], where a pathological case was considered. In the latter the physiological boundary conditions used were also taken from a previous reduced model simulation, and particular attention is devoted to the fluid flow pattern, wall shear stress and oscillatory shear index. In our work, besides reporting the quantities that influence the formation of several pathologies (i.e, the wall shear stress) we highlight some characteristics that are peculiar to the compliant wall simulations and validate the FSI model, such as the pulse wave velocity (PWV) and the radius change.

2 Model Description

While in many contexts the rheological properties of blood flow have a great influence on its dynamics, the flow in large healthy arteries is known to have an almost Newtonian behavior [11]. The interaction between the blood and the arterial wall has to be taken into account to correctly predict the behavior of the arteries, especially where the pressure impulse induces large deformations of the domain, as in the aortic arch. In the present work we will simulate the hemodynamics in the aorta, taking into account the 3D FSI between the blood

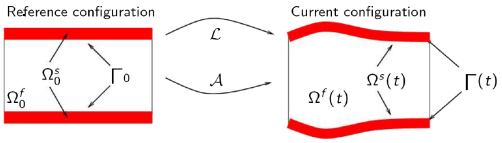

Figure 1: Reference and current configuration with Lagrangian and ALE mappings.

flow and the arterial wall, modeling blood as a Newtonian fluid and the aortic wall as a linear elastic structure. We recall in this section the model adopted in this work to describe the FSI problem, and the methodology used to solve it. We refer to [4] for further details.

The moving fluid domain is handled using the ALE formulation. This is a diffused approach in FSI, motivated by the need of imposing the boundary conditions for the fluid equations on an arbitrarily moving control volume, e.g. that follows the material configuration on the fluid-structure interface and is fixed at the inlet-outlet.

The FSI model considered is composed by three coupled subproblems. The *geometry problem*, introduced to define the ALE map, that describes the fluid domain displacement $\mathbf{d}_\mathrm{f}$ as a harmonic extension of the solid displacement $\mathbf{d}_\mathrm{s}|_{\Gamma_o}$ from the FS interface Γ_o to the internal of the fluid reference domain $\Omega_o^\mathrm{f} \subset \mathbb{R}^3$:

$$\begin{cases} -\Delta \mathbf{d}_\mathrm{f} &= 0 & \text{in } \Omega_o^\mathrm{f} \\ \mathbf{d}_\mathrm{f} &= \mathbf{d}_\mathrm{s}|_{\Gamma_o} & \text{on } \Gamma_o, \end{cases} \tag{2.1}$$

The ALE mapping is then defined as

$$\begin{aligned} \mathcal{A}_t : \Omega_o^\mathrm{f} &\rightarrow \Omega_t^\mathrm{f} \\ \mathbf{x}_o &\mapsto \mathcal{A}_t(\mathbf{x}_o) = \mathbf{x}_o + \mathbf{d}_\mathrm{f}(\mathbf{x}_o). \end{aligned}$$

The *fluid problem*, that consists of the incompressible Navier-Stokes equations written in ALE form

$$\begin{cases} \rho_\mathrm{f} \dfrac{\partial \mathbf{u}_\mathrm{f}}{\partial t}\bigg|_{x_o} + (\rho_\mathrm{f}(\mathbf{u}_\mathrm{f} - \mathbf{w}) \cdot \nabla)\mathbf{u}_\mathrm{f} - \nabla \cdot \sigma_\mathrm{f} = \mathbf{0} & \text{in } \Omega_t^\mathrm{f} \\ \nabla \cdot \mathbf{u}_\mathrm{f} = 0 & \text{in } \Omega_t^\mathrm{f}. \end{cases} \tag{2.2}$$

where $\sigma_\mathrm{f} = -pI + \mu(\nabla \mathbf{u}_\mathrm{f} + (\nabla \mathbf{u}_\mathrm{f})^T)$ is the Cauchy stress tensor, ρ_f is the blood density, μ is the dynamic viscosity and $\mathbf{u}_f$ and p represent blood velocity and pressure respectively.

The *solid problem* describes the arterial wall dynamics through a linear elastic model:

$$\rho_\mathrm{s} \frac{\partial^2 \mathbf{d}_\mathrm{s}}{\partial t^2} - \nabla \cdot \sigma_\mathrm{s}^o = 0 \text{ in } \Omega_o^\mathrm{s}, \tag{2.3}$$

where $\sigma_\mathrm{s}^o = \lambda \mathrm{tr}(\epsilon) + 2\mu_\mathrm{s}\epsilon$, with $\epsilon = \frac{(\nabla \mathbf{d}_\mathrm{s} + (\nabla \mathbf{d}_\mathrm{s})^T)}{2}$, is the Piola stress tensor and Ω_o^s is the solid domain in the reference configuration.

A wide variety of models for the structure of the arterial wall are present in literature, with different levels of complexity. An accurate model for the arterial wall should take into account the effects of anisotropy due to the distribution of the collagen fibers, the three layers (intima, media and adventitia) structure, the nonlinear behavior due to collagen activation and the incompressibility constraint. Accurate models devised for the tissue of the aorta, in particular applied to the study of pathological situations (abdominal aorta aneurisms (AAA), injuries), can be found e.g. in [14], [16] and more recently in [31], [29] and references therein. Furthermore, we refer to [15] for an overview of the mechanical properties of the arterial walls, and to [1] for an overview of the existing models and mathematical principles of the elasticity applied to the arterial wall. Needless to say the structural dynamics, and in particular the AAA formation, is greatly influenced by the patient specific geometry of the vessels, e.g. the eccentricity of the aorta lumen [9]. Also the physical parameters introduced in the model vary from case to case, influenced e.g. by the artery segment location and by the age of the patient, so that introducing complex models often requires extra parameter identifications.

The large arteries in healthy situations are often modeled with an isotropic linear elastic constitutive law in FSI applications. Although this constitutive relation is a rough simplification, the results by far improve those obtained using flow simulations with rigid walls, and show to correctly detect the hemodynamics (cf. Section 3.3). The Lamé coefficients λ and μ_s are characterized by the choice of a Young modulus and Poisson coefficient. In our simulations these are taken respectively as $E = 4\ 10^6 \frac{dyne}{cm^2}$ and $\nu = 0.48$, and the material is considered to be linear elastic. The viscosity of blood is set to $\mu = 0.035P$ [22].

Using the notations introduced in [4] we express, at a fixed time t, the equations describing the coupled problem in a compact form:

$$\begin{cases} \mathsf{G}(\mathbf{d}_s, \mathbf{d}_f) = 0 \\ \mathsf{F}(\mathbf{u}, \mathbf{d}_s, \mathbf{d}_f) = 0 \\ \mathsf{S}(\mathbf{u}, \mathbf{d}_s, \mathbf{d}_f) = 0, \end{cases} \tag{2.4}$$

where $\mathbf{u}$ represents the set of velocity and pressure unknowns in the Navier-Stokes equations, $\mathbf{d}_f$ is the fluid domain displacement and $\mathbf{d}_s$ is the structure displacement. We refer to [5] for the variational formulation of the coupled problem (2.4) which properly accounts for the coupling conditions on velocity and stresses. In the present work equations (2.4) are coupled using the *Geometry-Convective Explicit* (GCE) time discretization, i.e., considering in the fluid problem the fluid domain displacement explicitly and the convective term partly explicitly. With this choice of the time discretization the FSI system is linear at every time step, and the geometry problem can be solved in a separate step, leading to a significant reduction of the computational cost per time step with respect to other schemes, like the *convective explicit*, or the *fully implicit* ones (both with implicit treatment of the fluid geometry, see e.g. [18]). In [3] a similar coupling algorithm is used, but the fluid domain displacement is treated

implicitly and the GCE matrix is used as an approximation of the Jacobian in the Newton iterations, leading to an inexact Newton scheme where the *shape derivatives* are neglected.

The numerical simulations reported in the present work are performed using the FSI solver implemented in LifeV[1]. The fluid problem is discretized in space using P1-P1 finite elements stabilized with the interior penalty technique described in [24]. The solid and the geometry problems are discretized in space with P1 finite elements. The discretization in time is implicit Euler for the fluid (in its non conservative formulation, see [23]) and a Newmark second order scheme for the structure (see [23] Chap. 4).

3 Numerical Simulations

3.1 Geometry and Mesh

The geometric model of the aorta is obtained through 3T MRI scanner (Siemens Trio-Tim 3T System), details on the sequences used are mentioned in [27]. The arterial geometry was reconstructed in 3-D from the raw medical images (ITK Snap).

The structure part is obtained extruding the fluid surface in the normal direction. The thickness of the structure is proportional to the local aortic lumen, see [20]. An unstructured tetrahedral mesh was then generated with Gambit for both the fluid and the structure domains, conforming at the fluid-structure interface.

3.2 Boundary Conditions

The proper choice of the boundary conditions is essential to obtain simulations of physiological interest.

The simulation of a vessel subject to a high load, as it is the case in the thoracic aorta, undergoes large deformations concerning both the luminal radius and the vessel centerline displacement. In particular in a curved vessel, when imposing a free stress condition on the external wall, the movement of the domain turns out to be non physiological, as if there was no surrounding tissue around the solid wall. The importance of considering the surrounding tissue effects is often neglected, although in some cases it is shown to significantly change the behavior of the solution (e.g. [21]). Furthermore, as we will show, taking into account the surrounding tissue through a simplified model can be easily implemented in our numerical simulations. In absence of a constitutive law for the heterogeneous tissues surrounding the aorta, and to obtain a simple model for the external response, we assume a linear algebraic stress displacement constitutive relation on the external wall. This choice is arbitrary, but it leads to good agreement with the experiments, when we properly tune the coefficients in

[1] http://www.lifev.org

the constitutive law. The issue of the influence that the surrounding tissue has on the arterial hemodynamics was recently investigated in-vivo and in-vitro on swines [21]. In the latter work, under the physiological range for pressure and displacement, the intraluminal pressure was shown to be proportional to the radius of the lumen only when the surrounding tissue was taken into account, which suggests indeed a pressure-displacement linear constitutive relation.

More precisely, the boundary condition on the external wall is:

$$p_o\mathbf{n} + (\sigma^s \cdot \mathbf{n}) + \alpha\mathbf{d}_\mathrm{s} = 0 \text{ on } \Gamma_o, \tag{3.5}$$

where σ^s is the structure stress tensor, p_o is a static pressure and $\mathbf{n}$ is the outward normal to Γ_o. This is a Robin condition (see [25]). It is worth noticing that if we do not impose Neumann conditions on any other fluid and solid boundary, then the stresses σ^f and σ^s in the fluid and solid equations are defined up to a constant, which allows us to set $p_o = 0$ in the condition (3.5), and then to arbitrarily shift the pressure scale in the final solution.

The main difficulty encountered was a suitable choice of the parameter α in (3.5). We choose empirically for this parameter the value of $\alpha \approx 10^4 \frac{dyne}{cm^3}$, which leads to physiological displacements and fits qualitatively the plot of intraluminal pressure versus inner radius reported in [21]. However, as the wall thickness varies according to the intraluminal radius, we observed a great dilatation in the small branches when subject to a high intraluminal pressure. This dilatation would be avoided with a nonlinear structure model where the effects of collagen are taken into account. Our "remedy" to this problem has been to choose a parameter α varying in space, in particular increasing when the arterial wall becomes thin.

Another crucial issue concerning the imposition of boundary conditions on the arterial wall is the choice of the boundary conditions for the rings at the ends of the arterial branches. In fact, in the literature many strategies to impose absorbing boundary conditions on the fluid outlets have been devised. These allow in FSI to absorb the non physiological pressure wave reflections [23, 11]. However an absorbing boundary condition on the fluid outlets inhibits the imposition of other physiological quantities such as velocity, or stresses. Concerning the structure, at the best of our knowledge absorbing boundary conditions for FSI have not been implemented yet, thus we chose in our simulations to impose a Neumann homogeneous condition on the structure outflow rings. With this choice we did not observe spurious reflection waves. The aorta inlet in proximity of the aortic valve is clamped.

On the fluid outlets we impose fluxes obtained from 1D model simulations, as defective boundary conditions [10]. At the inlet we impose either the measured flux or a pressure obtained from the 1D simulation.

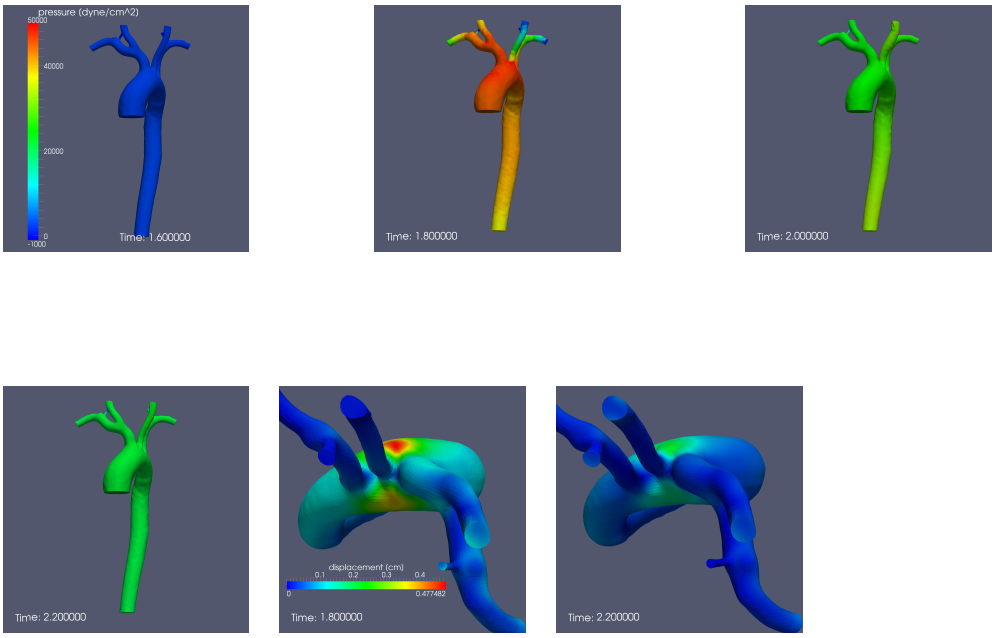

Figure 2: Pressure and displacement distribution at different times. The upper-left figure represents the pressure at the end of the second heartbeat (at $t = 1.6s$). The other pictures are taken at intervals of $0.2s$. We remark that the pressure reaches the maximum value in proximity of the systole, at $t \approx 1.8s$. The low-left and low-right figures represent the displacement magnitude at $t = 1.8s$ and $t = 2.2s$. The location of the maximum displacement during systole in the aortic arch is probably due to the curved and branching shape of the geometry inducing a variation of the eccentricity of the lumen.

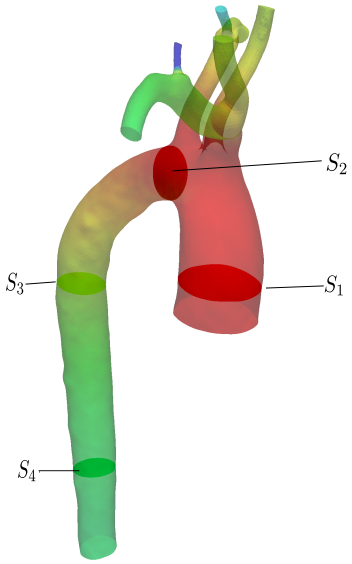

Figure 3: Sections in which the mean values of pressure and velocity are computed.

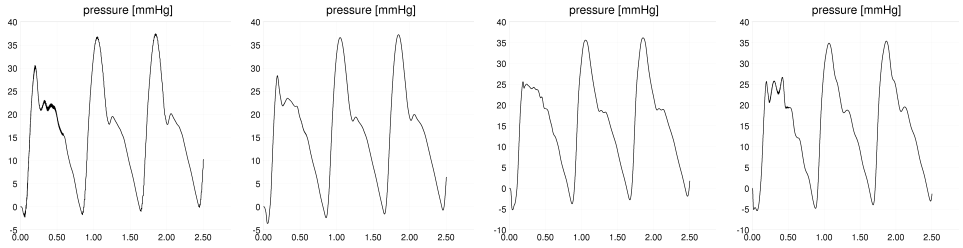

Figure 4: FSI simulation with inlet flux imposed. History of the mean pressures (in $mmHg$) at S_1, S_2, S_3 and S_4 in figure 3 (starting from the upper-left corner with the S_1 section, until the S_4 section in the low-right corner).

3.2.1 FSI vs Rigid Walls

In order to compare our results with a standard Navier-Stokes simulation with rigid walls we set up a CFD problem with similar boundary conditions as those imposed in the previously described simulations. Thus we keep the imposition of the fluxes at all the outlets, and we substitute the inlet flux with a constant normal stress condition on the inlet section. Note that as the inlet is the only boundary where a Neumann condition is imposed, the value of the stress imposed is defined only up to a constant.

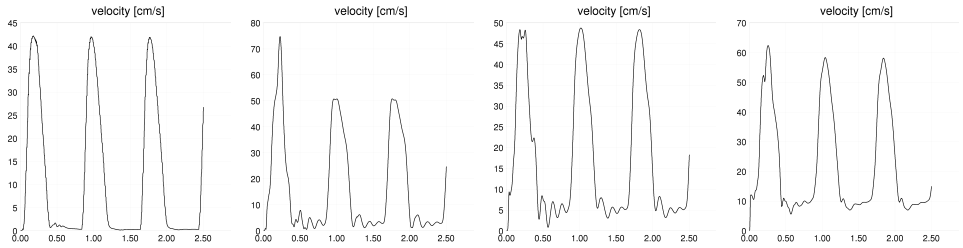

Figure 5: FSI simulation with inlet flux imposed. Mean velocities computed in the sections S_1, S_2, S_3 and S_4 represented in figure 3.

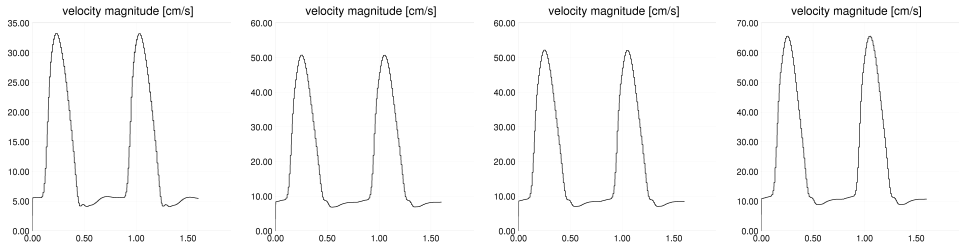

Figure 6: NS simulation with rigid walls. History of the mean velocity over the sections S_1, S_2, S_3 and S_4 represented in figure 3, starting from the S_1 section (up left), until the abdominal outflow S_4 (low right). The imposition of an inlet pressure instead of a flux leads to a nonzero positive flux through the aortic valve (section S_1) also when the valve should be closed.

3.3 Timings and Validation

All the simulations reported in this paper were run using the parallel FE library LifeV[2]. The computations were done on the massively parallel processing Cray XT4 supercomputer *HECToR*[3], composed by blades containing 4 quad-core (AMD 2.3 GHz) nodes each. LifeV uses the Trilinos[4] library as interface to MPI. All the simulations were run on 16 nodes using 4 MPI processes per node. At every time-step most of the time was spent in the preconditioner computation, in the solution of the linear system, and in the assembly of the matrix block for the fluid equations. The average time for these tasks was $16.6s$, $11.5s$ and $8.1s$ respectively (the assembly of the stabilization part at every time iteration took $7.1s$, while the assembly of the rest of the block took about $1s$). The preconditioner considered was a one-level algebraic additive Schwarz (AAS) preconditioner with two layers overlap (see [26]). The LU factorization of the sub-blocks in the AAS preconditioner was achieved through the unsymmetric

[2]http://www.lifev.org
[3]http://www.hector.ac.uk
[4]http://trilinos.sandia.gov

multifrontal method implemented in the package Umfpack[5]. The linear system was solved with preconditioned GMRES iterations and the average number of iterations was about 25. The time-step chosen was $10^{-3}s$, so that one heartbeat ($0.8s$) consisted of 800 time levels. Summing the timings for the solution of the linear system, the preconditioner computation and the assembly of the fluid block we obtain a global timing per heartbeat of about 8 hours. However by also considering the Hdf5 post-processing at every time-step this time increases to about $10h$. Neglecting the post-processing time we remark that the assembly of the fluid block scales while increasing the number of processors since it does not require inter-processor communications (the *ghost nodes* of each partition are repeated on all the processors), while the preconditioner computation, and in particular the GMRES solution, are less scalable operations. We refer to [4] for considerations on the scalability of the FSI GCE system and for a discussion on suitable preconditioners for coupled problems.

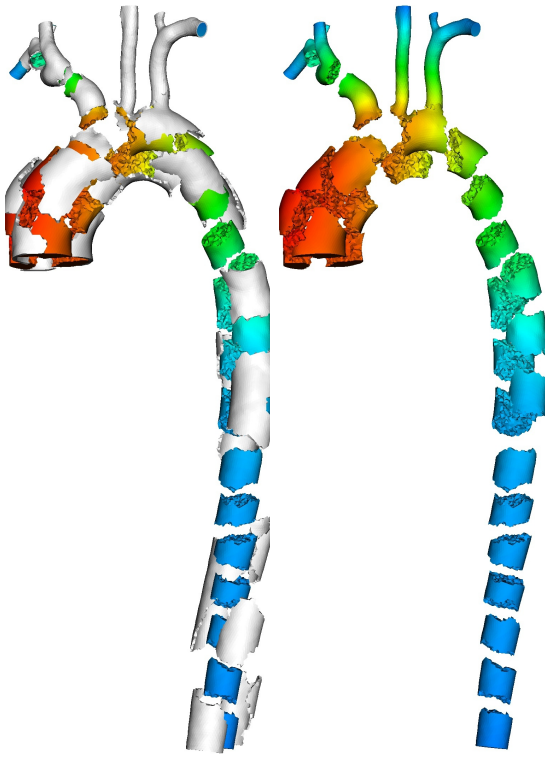

Figure 7: Aorta mesh partitioned with 32 processors. The mesh is composed of $380'690$ tetrahedra, i.e., $324'000$ dofs.

[5]http://www.cise.ufl.edu/research/sparse/umfpack

The velocity of the pressure wave is measured by evaluating the foot of pressure in two sections of the abdominal aorta $5cm$ from each other. The phase shift observed is $0.009s$, which corresponds to a velocity of $5.5\frac{m}{s}$. This value corresponds to the physiological PWV (around $5\frac{m}{s}$, see [22], [12]). However this value is closely related to the Young modulus chosen in the solid model, which depends on the specific case and is influenced by many factors. For patient specific simulations these parameters should be accurately tuned. Furthermore, frequently the Young modulus for in-vivo arteries is devised from the PWV using empirical formulas, or from measurements of pressure versus luminal area, thus already taking into account the effect of the surrounding tissue [21].

To test the influence of the flux boundary condition imposed at the inlet and to have another comparison with the rigid walls simulation, we ran an FSI simulation imposing the pressure at the inlet obtained from a 1D model simulation. With this choice we do not guarantee that the flux is zero when the aortic valve is closed. We observe indeed a reflux in the diastolic phase, that simulates the back flow inducing the closure of the aortic valve and the flow into the coronary arteries. This phenomenon is physiologically observed and cannot be simulated without taking into account the compliance of the wall. However imposing a stress condition at the inlet introduces another parameter to be tuned. In fact the outer static pressure p_o, that we set to zero in (3.5), in this case is no more arbitrary. The value chosen is $p_o = 115000dyne \approx 86mmHg$, which is slightly greater than the diastolic inlet pressure.

The time histories of the mean pressure and normal velocity computed on the sections represented in Figure 3 are reported in Figures 8 and 9, where only the second heartbeat is represented. Note that instead of imposing the external static pressure p_o we shifted the inlet pressure so that the zero value corresponds to $p_o \approx 86mmHg$. Figure 12 represents a section of the lumen boundary in the middle of the aortic arch at different times, showing in particular the change in eccentricity of the lumen.

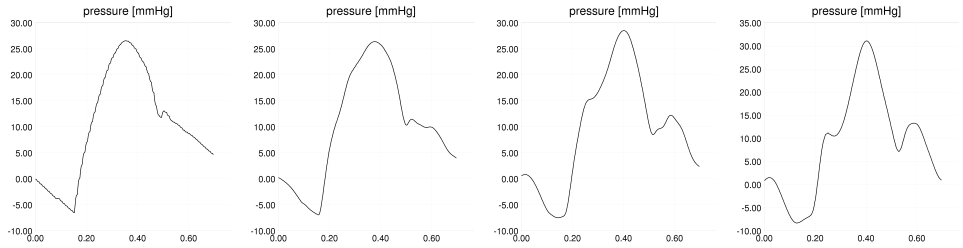

Figure 8: FSI simulation with inlet pressure imposed. History of the mean pressures (in $mmHg$) over the sections S_1, S_2, S_3 and S_4 represented in figure 3.

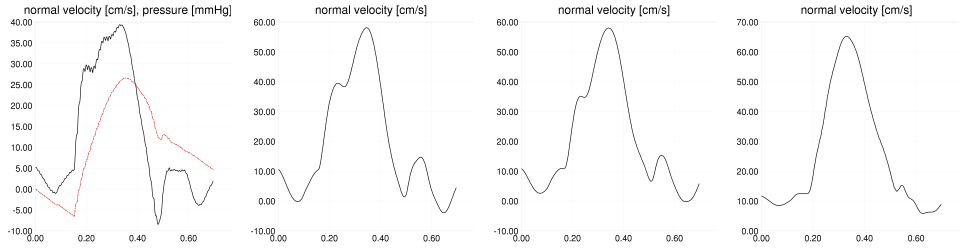

Figure 9: FSI simulation with inlet pressure imposed. History of the mean normal velocities (in cm/s) over the sections S_1, S_2, S_3 and S_4 represented in Figure 3. In the plot for the S_1 section (upper-left) we show the pressure curve over the same section with a dashed line, to highlight the dependence of the reverse flow in the coronary arteries on the steep pressure decrease after the systole. Notice that at regime in the abdominal aorta no more backward flow is observed.

4 Wall Shear Stress

The arterial wall tissue reacts to both the normal and shear stresses [11]. In particular, the wall shear stress is involved with the formation of atherosclerosis, which is a pathology which is characterized by a narrowing of the arterial lumen due to the accumulation of fatty material. However wall shear stress is difficult to measure in vivo with a sufficient spatial resolution. Thus numerical simulations can help to predict the WSS distribution in a specific geometry of the vessel, improving diagnosis and prevention. A reliable numerical tool that carries out all the process from the patient-specific segmentation to the simulation could help a medical doctor to choose the correct therapy adapted to a specific patient. Furthermore, if the model is validated, a simulation of the WSS distribution can help to solve the inverse problem, i.e., to identify the role that WSS plays in the

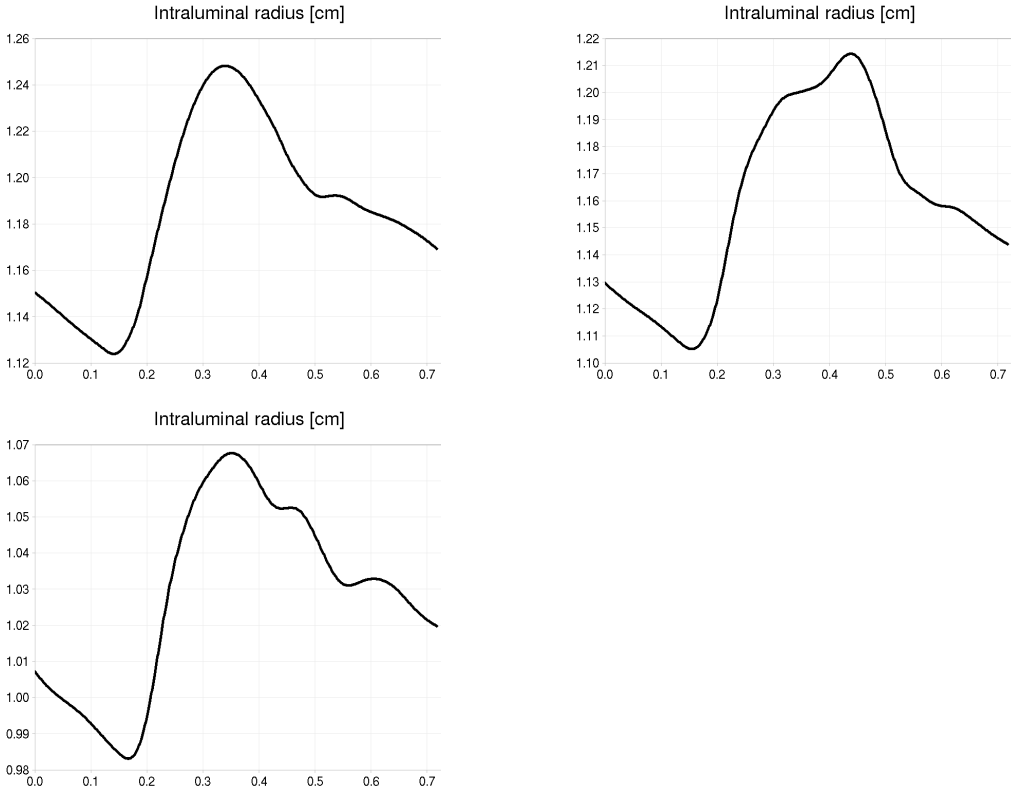

Figure 10: History of the mean radius over the sections S_2, S_3 and S_4 represented in figure 3, for the simulation with inlet flux imposed.

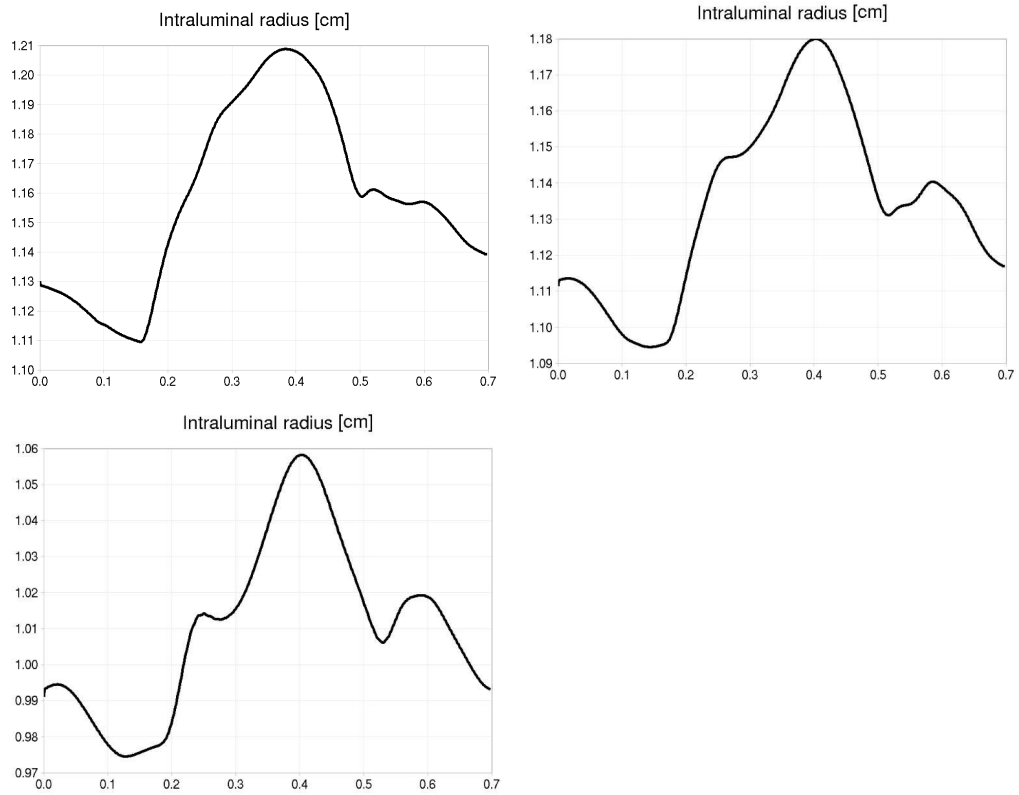

Figure 11: History of the mean radius over the sections S_2, S_3 and S_4 represented in figure 3 for the simulation with inlet pressure imposed.

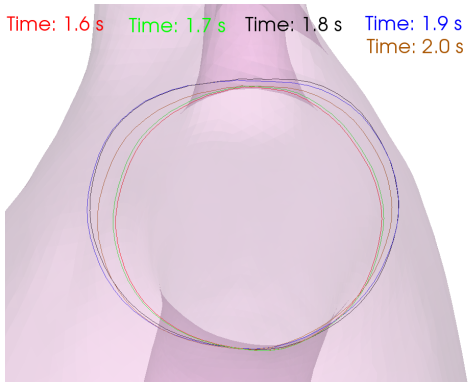

Figure 12: Several snapshots of the aorta section located in the middle of the aortic arch during the third heartbeat of the inlet flux FSI simulation.

development of pathologies such as atherosclerosis.

The shear stress is defined as the tangential component of the traction vector $\sigma_f \mathbf{n}$. Thus in Newtonian fluids it is

$$\boldsymbol{\tau} = \sigma_{\mathrm{f}}\mathbf{n} - (\sigma_{\mathrm{f}}\mathbf{n}\cdot\mathbf{n})\mathbf{n} = \mu(\nabla\mathbf{u}_{\mathrm{f}} + \nabla\mathbf{u}_{\mathrm{f}}^T)\mathbf{n} - \mu\{[(\nabla\mathbf{u}_{\mathrm{f}} + \nabla\mathbf{u}_{\mathrm{f}}^T)\cdot\mathbf{n}]\cdot\mathbf{n}\}\mathbf{n}$$

where μ is the dynamic viscosity. If $\mathbf{u}_{\mathrm{f}} = (u_1, u_2, u_3)$ the latter corresponds to

$$\boldsymbol{\tau} = \mu[(\nabla\mathbf{u}_{\mathrm{f}} + \nabla\mathbf{u}_{\mathrm{f}}^T) - (\nabla\mathbf{u}_{\mathrm{f}} + \nabla\mathbf{u}_{\mathrm{f}}^T) : (\mathbf{n}\otimes\mathbf{n})]\mathbf{n}.$$

Written in Einstein notation the latter reads

$$\tau_j = \mu[(\partial_i u_j + \partial_j u_i) - (\partial_k u_l + \partial_l u_k)(n_k n_l)\delta_{ij}]n_i.$$

Fixing a point $\mathbf{x}$ on the fluid-structure interface we can write all the quantities with respect to the associated frame of reference $(\mathbf{t}_1, \mathbf{t}_2, \mathbf{n})$, where $\mathbf{t}_1$ and $\mathbf{t}_2$ are orthonormal vectors on the tangent plane and $\mathbf{n}$ is the normal vector. We denote the local coordinate system associated with this frame (ξ_1, ξ_2, ξ_3). The previous expression reads

$$\boldsymbol{\tau} = \mu \begin{pmatrix} (\partial_{\xi_2} u_{\xi_3} + \partial_{\xi_3} u_{\xi_2}) \\ (\partial_{\xi_1} u_{\xi_3} + \partial_{\xi_3} u_{\xi_1}) \\ 0 \end{pmatrix}.$$

We notice here that if the FS wall is fixed every tangential derivative is zero, $\partial_{\xi_1} u_{\xi_3} = 0$, $\partial_{\xi_2} u_{\xi_3} = 0$. This leads to a straightforward relation between the magnitude of the wall shear stress and of the vorticity vector $\boldsymbol{\omega} = \nabla \times \mathbf{u}_{\mathrm{f}}$. In fact we have that

$$\boldsymbol{\omega} = \begin{pmatrix} \partial_{\xi_2} u_{\xi_3} - \partial_{\xi_3} u_{\xi_2} \\ \partial_{\xi_3} u_{\xi_1} - \partial_{\xi_1} u_{\xi_3} \\ \partial_{\xi_1} u_{\xi_2} - \partial_{\xi_2} u_{\xi_1} \end{pmatrix} = \begin{pmatrix} -\partial_{\xi_3} u_{\xi_2} \\ -\partial_{\xi_3} u_{\xi_1} \\ 0 \end{pmatrix}$$

and thus $\mu\|\boldsymbol{\omega}\|_2 = \|\boldsymbol{\tau}\|_2$.

When the wall is moving this relation is no longer valid. However in the following we suppose that the velocity gradient due to the boundary layer (the normal derivatives of the tangential velocity) dominates the other components of the velocity gradient, so that $\mu\|\boldsymbol{\omega}\|_2 \approx \|\boldsymbol{\tau}\|_2$. We refer to [30] for details and discussions about shear stress and vorticity relations.

Figures 14 and 13 show the wall shear stress (WSS) magnitude in both the rigid walls and FSI simulations computed through the wall vorticity right after the systole of the second heartbeat. The period of one heartbeat is $T = 0.8s$, so that $t = 1s$ corresponds approximatively to the systolic peak. The WSS distribution is similar at systole with rigid walls and FSI, although it is slightly larger in the former case, then at $t = 1.1s$ and $t = 1.2s$ the WSS magnitude is larger in the rigid walls case. In particular the WSS in the rigid wall

simulation seems to be overestimated, we refer to [28] for a detailed comparative study of the two simulations. The systolic WSS are in the physiological range, particularly in the FSI case, if compared with measurements obtained in [2] for the control patients. We did not observe remarkable differences between the two FSI simulations corresponding to different inlet boundary conditions.

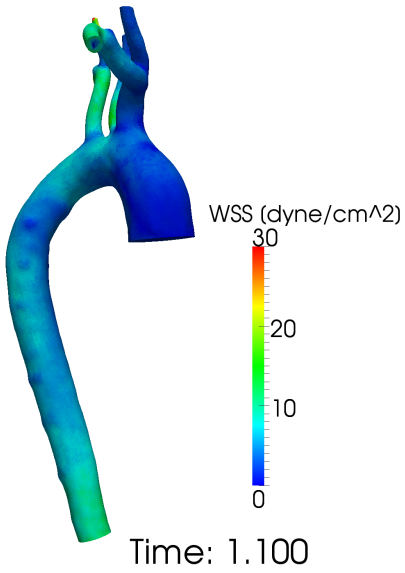

Figure 13: The wall shear stress distribution at $t = 1.1$ for the FSI simulation with the inlet flux imposed.

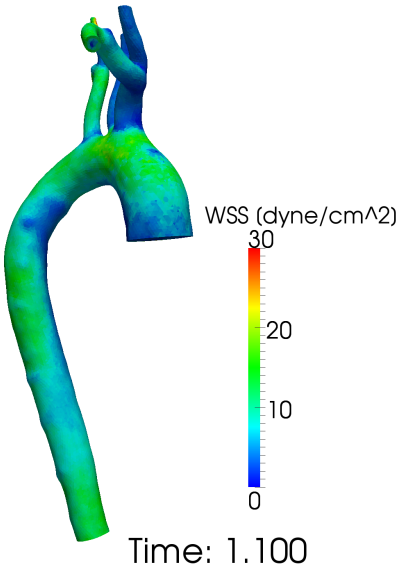

Figure 14: This figure represents the wall shear stress distribution at $t = 1.1$ for the rigid walls simulation.

5 Conclusions

In this paper we report the result of 3D simulations on a physiological geometry over several heartbeats. We tested different boundary conditions at the inlet in proximity of the aortic valve. In particular we ran a simulation imposing a measured flux at the inlet section and fluxes obtained from a 1D simulation on all the outlets. We then imposed an inlet pressure instead of the flux, and observed a backward diastolic flow through the section. This phenomenon is observed and causes the closure of the aortic valve and the circulation in the coronary arteries. Since it is due to the compliance of the arterial wall it cannot be simulated using only a CFD code that does not take into account the fluid-structure interaction.

We introduced a Robin condition at the external wall to take into account the influence of the heterogeneous tissue surrounding the aorta. This condition consists of a pressure-displacement linear relation, that when properly tuned leads to results that agree with physiological ones. To validate our model we computed the pulse wave velocity, wall shear stress, the histories of the mean pressure, velocity and intraluminal radius at different axial sections along the vessel. We found that the values are in the physiological range, though many parameters may be adapted on a patient-specific basis.

We compared the FSI results with those obtained through a CFD simulation with rigid walls in which the pressure is imposed at the inlet section. In particular we observed a difference in the wall shear stress magnitude, that is overestimated with rigid wall. Furthermore we observed a flux entering through the inlet section

in the rigid wall simulation also when the valve is closed, while there should be a reflow inducing the closure of the aortic valve, which is indeed observed in the FSI case. We stress the fact that in the FSI model we could impose fluxes over every inlet and outlet of the arterial tree, which would not be possible in a rigid wall simulation, as well as in many FSI codes (see [19]), unless the Dirichlet condition on the fluid-structure interface would be substituted with another proper condition.

Acknowledgments

We acknowledge the support provided by the Swiss National Science Foundation under grant 200020-117587 and the European Research Council Advanced Grant "Mathcard, Mathematical Modelling and Simulation of the Cardiovascular System" Project ERC-2008-AdG 227058. Support has also been provided by the VPH2 project FP7 224635, and by the DEISA Consortium (www.deisa.eu), co-funded through the EU FP7 project RI-222919, under the DEISA Science Community support programme. This work was also supported by the by the European Commission contract no. IST-027703 @neurIST Project and by the Center for Biomedical Imaging (CIBM) of the Geneva-Lausanne Universities, the EPFL and the University Hospitals of Geneva and Lausanne.

References

[1] D. Balzani. *Polyconvex Anisotropic Energies and Modelling of Damage Applied to Arterial Wall*. PhD thesis, 2006.

[2] A. J. Barker, C. Lanning, and R. Shandas. Quantification of hemodynamic wall shear stress in patients with bicuspid aortic valve using phase-contrast mri. *Ann Biomed Eng*, 2009.

[3] Y. Bazilevs, J. Gohean, T. Hughes, R. Moser, and Y. Zhang. Patient-specific isogeometric fluid-structure interaction analysis of thoracic aortic blood flow due to implantation of the Jarvik 2000 left ventricular assist device. *Computer Methods in Applied Mechanics and Engineering*, 198(45-46):3534 – 3550, 2009.

[4] P. Crosetto, S. Deparis, G. Fourestey, and A. Quarteroni. Parallel solvers and preconditioners for fluid-structure interaction problems arising in haemodynamics. submitted.

[5] S. Deparis, M. Discacciati, G. Fourestey, and A. Quarteroni. Fluid-structure algorithms based on Steklov-Poincaré operators. *Comput. Methods Appl. Mech. Engrg.*, 195(41-43):5797–5812, 2006.

[6] S. Deparis, M. A. Fernández, and L. Formaggia. Acceleration of a fixed point algorithm for fluid-structure interaction using transpiration conditions. *M2AN Math. Model. Numer. Anal.*, 37(4):601–616, 2003.

[7] T. Fanion, M. Fernández, and P. L. Tallec. Deriving adequate formulations for fluid structure interaction problems: from ale to transpiration. *Rév. Européenne Élém. Finis*, 9(6-7):681–708, 2000.

[8] C. A. Figueroa, I. E. Vignon-Clementel, K. E. Jansen, T. J. Hughes, and C. A. Taylor. A coupled momentum method for modeling blood flow in three-dimensional deformable arteries. *Computer Methods in Applied Mechanics and Engineering*, 195(41-43):5685 – 5706, 2006. John H. Argyris Memorial Issue. Part II.

[9] P. M. Flynn, G. Sullivan, and A. S. Pandit. Geometric variability of the abdominal aorta and its major peripheral branches. *Ann Biomed Eng*, 38(3):824–40, 2010.

[10] L. Formaggia, J. F. Gerbeau, F. Nobile, and A. Quarteroni. Numerical treatment of defective boundary conditions for the Navier-Stokes equations. *SIAM Journal on Numerical Analysis*, 40(1):376–401, 2003.

[11] L. Formaggia, A. Quarteroni, and A. Veneziani, editors. *Cardiovascular Mathematics: Modeling and Simulation of the Circulatory System*, volume 1 of *Modeling, Simulation and Applications*. Springer, Milan, 2009.

[12] Y. C. Fung. *Biomechanics : circulation*. Springer, New York, 2nd ed edition, 1997.

[13] F. Gao, M. Watanabe, and T. Matsuzawa. Fluid-structure interaction within a layered aortic arch model. *Journal of Biological Physics*, 32(5):435–454, 2006.

[14] G. Holzapfel, T. Gasser, and R. Ogden. A new constitutive framework for arterial wall mechanics and a comparative study of material models. *Journal of Elasticity*, pages 1–48, 2000.

[15] G. A. Holzapfel and R. W. Ogden. *Mechanics of Biological Tissue*. Springer Verlag, 2006.

[16] G. A. Holzapfel, M. Stadler, and C. A. J. Schulze-Bauer. A layer-specific three-dimensional model for the simulation of balloon angioplasty using magnetic resonance imaging and mechanical testing. *Annals of Biomedical Engineering*, 30(6):753–767, 2002.

[17] H. Kim, I. Vignon-Clementel, C. Figueroa, J. LaDisa, K. Jansen, J. Feinstein, and C. Taylor. On coupling a lumped parameter heart model and a three-dimensional finite element aorta model. *Ann Biomed Eng.*, pages 2153–69, 2009.

[18] U. Küttler, M. Gee, C. Förster, A. Comerford, and W. A. Wall. Coupling strategies for biomedical fluid–structure interaction problems. *Commun. Numer. Meth. Engng.*, 2009.

[19] U. Küttler and W. A. Wall. The dilemma of domain decomposition approaches in fluid-structure interactions with fully enclosed incompressible fluids. In *Domain decomposition methods in science and engineering XVII*, volume 60 of *Lect. Notes Comput. Sci. Eng.*, pages 575–582. Springer, Berlin, 2008.

[20] G. J. Langewouters. *Visco-Elasticity Of The Human Aorta In Vitro In Relation To Pressure And Age*. PhD thesis, Free University, Amsterdam, 1982.

[21] Y. Liu, C. Dang, M. Garcia, H. Gregersen, and G. S. Kassab. Surrounding tissues affect vessel mechanics. *AJP - Heart and Circulatory Physiology*, (294):514–523, 2008.

[22] W. W. Nichols and M. F. O'Rourke. *McDonald's Blood Flow in Arteries Theoretical, experimental, and clinical principles*. Arnold, 1998.

[23] F. Nobile. *Numerical Approximation of Fluid-Structure Interaction Problems with Application to Haemodynamics*. PhD thesis, École Polytechnique Fédérale de Lausanne, 2001.

[24] N. Parolini and E. Burman. Subgrid edge stabilization for transport equations. Technical report, 2005. EPFL-IACS report 09.2005.

[25] A. Quarteroni. *Numerical Models for Differential Problems*, volume 3 of *Modeling, Simulation and Applications*. Springer, Milan, 2009.

[26] A. Quarteroni and A. Valli. *Domain Decomposition Methods for Partial Differential Equations*. Oxford Science Publications, Oxford, 1999.

[27] P. Reymond, Y. Bohraus, F. Perren, F. Lazeyras, and N. Stergiopulos. Validation of a person-specific 1-d model of the systemic arterial tree. In preparation.

[28] P. Reymond, P. Crosetto, D. Kontaxakis, S. Deparis, A. Quarteroni, and N. Stergiopulos. Physiological aspects of fluid structure interaction and their effects on blood flow in a person-specific aorta. In preparation.

[29] J. Rodriguez, C. Ruiz, M. Doblaré, and G. Holzapfel. Mechanical stresses in abdominal aortic aneurysms: Influence of diameter, asymmetry, and material anisotropy. *Journal of Biomechanical Engineering*, 130, 2008.

[30] J.-Z. Wu, H.-Y. Ma, and M.-D. Zhou. *Vorticity and Vortex Dynamics*. Springer, 1 edition, May 2006.

[31] A. R. Zhao, M. L. Field, K. Digges, and D. Richens. Blunt trauma and acute aortic syndrome: a three-layer finite-element model of the aortic wall. *European Journal of Cardio-Thoracic Surgery*, 34(3):623 – 629, 2008.

MOX Technical Reports, last issues

Dipartimento di Matematica "F. Brioschi",
Politecnico di Milano, Via Bonardi 9 - 20133 Milano (Italy)

28/2010 Paolo Crosetto, Philippe Reymond, Simone Deparis, Dimitrios Kontaxakis, Nikolaos Stergiopulos, Alfio Quarteroni:
Fluid Structure Interaction Simulations of Physiological Blood Flow in the Aorta

27/2010 Matteo Bruggi, Marco Verani:
An adaptive algorithm for topology optimization with goal-oriented error control

26/2010 Francesca Ieva, Anna Maria Paganoni:
Designing and mining a multicenter observational clinical registry concerning patients with Acute Coronary Syndromes

25/2010 G. Pena, C. Prud'homme, Alfio Quarteroni:
High Order Methods for the Approximation of the Incompressible Navier-Stokes Equations in a Moving Domain

24/2010 Lorenzo Tamellini, Luca Formaggia, Edie Miglio, Anna Scotti:
An Uzawa iterative scheme for the simulation of floating boats

23/2010 Joakim Baeck, Fabio Nobile, Lorenzo Tamellini, Raul Tempone:
Stochastic Spectral Galerkin and collocation methods for PDEs with random coefficients: a numerical comparison

22/2010 Carlo D'Angelo, Paolo Zunino:
Numerical approximation with Nitsche's coupling of transient Stokes'/Darcy's flow problems applied to hemodynamics

21/2010 Niccolo' Grieco, Francesca Ieva, Anna Maria paganoni:
Provider Profiling Using Mixed Effects Models on a Case Study concerning STEMI Patients

20/2010 Fabio Nobile, Alfio Quarteroni, Ricardo Ruiz Baier:
Numerical solution of an active strain formulation for the electro-mechanical activity in the heart

19/2010 Loredana Gaudio, Alfio Quarteroni:
hN-adaptive spectral element discretization of optimal control problems for environmental applications